

Nanostructured Li Ion Insertion Electrodes. 1. Discussion on Fast Transport and Short Path for Ion Diffusion

P. R. Bueno* and E. R. Leite

Interdisciplinary Laboratory of Electrochemistry and Ceramics, Department of Chemistry, Federal University of São Carlos, C. Postal 676, 13565-905 São Carlos, SP, Brazil

Received: February 27, 2003; In Final Form: June 6, 2003

This paper describes the mechanisms of ion and electron transport in nanostructured insertion electrode materials such as metal oxide electrochromics and/or Li ion batteries. A general description is given of cases of insertion into a short path region predicted by the geometric disposition of insertion materials in nanostructural electrodes, designed mainly by connected spherical-like particles and nanofibers, both protruding from the current collector substrate. The short path scheme for ion diffusion (nanometer length) permits an ion storage mechanism to be treated as a capacitance charge rather than a diffusion process, an effect that is dubbed the “nanoscale effect”. As a result of heterogeneous charge-transfer resistance, the intercalation sites may be seen as the occupation of an ion immobilized-like state. A scheme of an ion trapping-like state represents, in the present case, an ion-binding process occurring during the intercalation reaction, like Li^+ forming a bond to a bridging-type oxygen in metal oxide based insertion materials. The model predicts a relaxation process for the intercalation reaction which is more clearly visible in cases of fast transport (occurring throughout the solid and liquid/electrolyte phases of a nanosized macrohomogeneous medium) and/or high state-of-charge. The characteristic frequency of this relaxation process can be used to predict the rate of Li ion intercalation reaction in different nanosized host materials.

I. Introduction

Nanoscale materials for lithium ion storage devices or electrochromic windows¹ are emerging as successful solutions to improve the rate capability, which, in the case of lithium ion insertion batteries, focuses on anodes and cathodes.²

A battery's rate capability is its ability to deliver a large capacity when discharged at high C rates (a rate of $C/1$ corresponds to the current required to completely discharge an electrode in 1 h). During high-power pulses required for transmission of digitized and compressed voice data, the battery's delivery capacity decreases to a fraction of its low-rate value. It is widely believed that these limitations in the rate capabilities of Li ion batteries are caused by slow solid-state diffusion of Li^+ within the electrode materials.^{2–6} For this reason, tremendous interest currently focuses on the research and development of nanostructured Li ion battery electrodes, whose nanostructure clearly restricts the distance that Li^+ must diffuse, which may be as small as 50 nm.

Two kinds of geometry are commonly applied to achieve a faster solid-state diffusion, as depicted in Figure 1, the first based on connected spherical-like nanoparticle nanofibers and the second based on nanofibers that protrude, brushlike, from the current collector; in fact, this type of nanostructured electrode geometry allows for improved rate capabilities.^{1,3–6}

Although the possibilities of this complex situation involving the movement of Li^+ ions and electrons through different nanostructured media have not all been adequately exploited to offer predictable ways of designing a wide range of novel Li^+ ion insertion electrodes, the topic of electronic and ionic transport in complex configurations, including that schematically

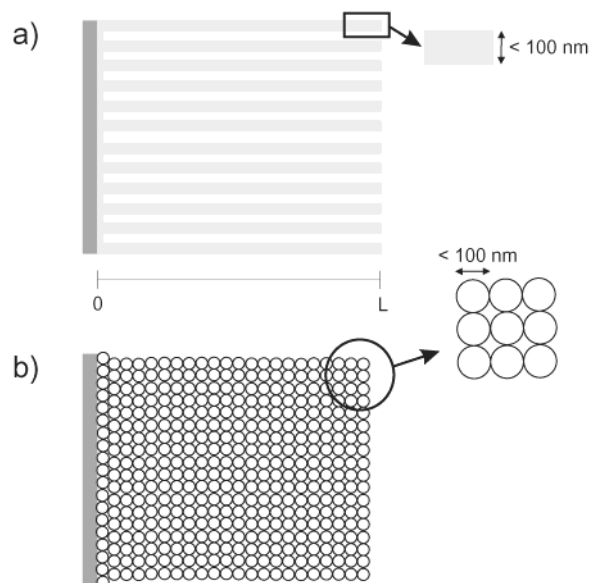


Figure 1. Schematic representation of a highly porous structure of nanostructured electrode materials protruding from a current collector. (a) Nanofiber structure or a templatelike membrane and (b) spherical-like particle-based nanostructure. Note that real nanostructures are not so regular, but both the nanostructured phase and electrolyte, as discussed herein, are continuous along the length L .

presented in Figure 1, shows that this transport can be modeled similarly, provided a macrohomogeneous description of two closely mixed phases is used.⁷ Thus, the macrohomogeneous concept⁷ is useful to generalize different electrodes involving nanosized insertion materials.

A good approach to study the kinetics of the Li ion insertion reaction into nanostructured electrodes is provided by frequency-

* To whom correspondence should be addressed. E-mail: paulo@iris.ufscar.br.

resolved techniques. These techniques can be used as a powerful tool to monitor the fundamental changes in steady-state conditions, especially in cases where a macrohomogeneous scheme arises similar to, for instance, that depicted in Figure 1.

Therefore, the electrode's nanostructure is composed of two mixed phases: (i) a solid phase having the form of connected channels of spherical-like particles or nanofibers that protrude from the current collector substrate and (ii) a liquid phase consisting of a penetrating electrolyte that reaches the current collector substrate. In specific cases in which a solid electrolyte is used, this macrohomogeneous medium can be seen as a mixture of two solid phases without compromising the result of the analysis. It should be noted that if the percolating phase emerging from the current collector substrate is primarily a mixed ionic and electronic conductor, on the other hand, the other phase (such as a liquid) that emerges from the electrolyte (which can be seen as an ion collector penetrating up to the current collector substrate) must be a purely ionic conductor.

Furthermore, because of the previous picture, the transmission line approach is easily used to envision a physical model based on frequency-dependent phenomena. In the particular case of nanostructured electrodes, as previously discussed, a physical model describing the main processes involved in a nanostructured electrode must consider the "nanoscale effect", which can be seen, in principle, as the overcoming of the restriction for Li ion diffusion through the solid phase in the frequency domain due to the short path that Li ion takes for diffusion. This primary feature of nanostructure-based electrode materials is called the "nanoscale effect" throughout this paper. In fact, this effect is very important in understanding the frequency-dependent response observed in several Li ion nanostructured insertion electrodes. In this paper, we present the most likely responses expected to arise from frequency-dependent responses when the "nanoscale effect" is present, with emphasis on the responses in which the charge carrier density in the liquid phase is sufficiently high to decrease their resistance to values that do not respond to the oscillating perturbation or, in other words, when there is no potential drop in the channel or in the thickness of the layer (see Figure 2b).

In the above description, the "nanoscale effect" can be evaluated because it acts in such a way that Li^+ ion diffusion into the structure of the host materials must, in fact, be treated as a pure capacitive element in the frequency domain response. Therefore, a "truly" ion trapping dynamics is formed between Li^+ present in the double layer surface and Li^+ intercalated in solid state sites. Moreover, if different intercalation sites exist in the bulk of nanocrystalline materials, distinct charging modes are expected to arise. Due to this fact, the ion intercalation dynamics can be treated according to the lattice-gas model.⁸⁻⁹ Thus, tetragonal and octahedral sites commonly available for intercalation in crystalline structures, for instance, could be treated as two separate trapping states (or immobilized sites for ions) with different energies for intercalation. A nanosized insertion material possessing two distinct crystalline phases could also be treated similarly. An analysis of some consequences of the "nanoscale effect" on the frequency response of the nanostructured electrodes will be discussed in this paper.

II. Transmission Line Model Approach of a Macrohomogeneous Medium

The classical porous electrode theory⁸ can be applied to different situations,¹¹ for example, in the analysis of nonfaradaic or faradaic processes inside a porous electrode, considered as a macrohomogeneous mixture of two phases,⁷ as briefly discussed

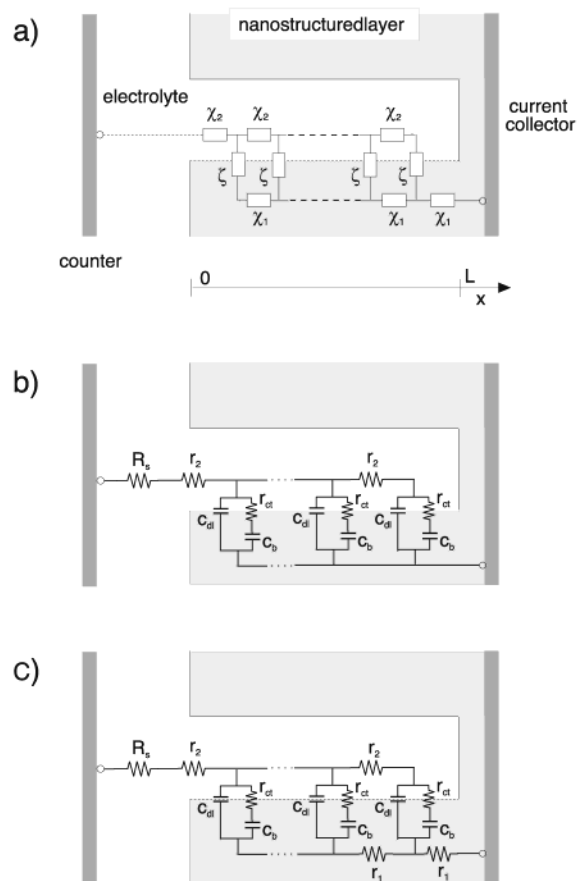


Figure 2. Schematic representation of the inner region $0 < x < L$ of a nanostructured electrode consisting of a porous film deposited on a conducting substrate. The dashed line represents the solid/liquid interface inside the pores. (a) The generalized equivalent circuit model corresponding to eq 1. (b) The particular configuration representing the nanostructure-based electrode for high electronic conductivity in the solid phase, according to the model discussed here. (c) The particular configuration representing the nanostructure-based electrode when neither the liquid nor the solid phase is a good ionic or electronic conductor. For the model to be applied to the actual geometry of the electrode, the nanostructure does not have to be as regular as the one depicted here, but each phase must be continuous throughout the electrode's length.

in the previous section. For the argument development in this paper, it is more convenient to consider a macrohomogeneous medium of a solid (connected spherical-like nanoparticles or nanofiber-based scheme, as depicted in Figure 1) and a liquid phase (connected porous structure filled with an electrolyte). Therefore, we have assumed that our electrode has the configuration of a porous electroactive film deposited on a conductive substrate, which is dipped into a liquid electrolyte that fills the connected chain of pores, to reach the substrate contact. In this scheme (see Figures 1 and 2 for details), different species (electronic and ionic) can be conducted through the macrohomogeneous medium, but with the macroscopic boundaries possibly being impermeable to different species; for example, an electron coming from the solid phase cannot penetrate into the liquid phase. Thus, solid/liquid interfaces in the porous channel are impermeable to electrons but not to ions, which, in specific cases, can penetrate into the solid phase.

According to the boundary conditions previously described, the macrohomogeneous medium is represented in Figure 2a in a generalized transmission line impedance approach, in which the faradaic currents and polarization may occur on the inner surface that separates the two phases, solid and liquid. The impedance

function to this generalized dual-channel transmission line model is given by the following expression:

$$Z = \frac{\chi_1 \chi_2}{\chi_1 + \chi_2} \left(L + \frac{2\lambda}{\sinh(L/\lambda)} \right) + \lambda \frac{\chi_1^2 + \chi_2^2}{\chi_1 + \chi_2} \coth(L/\lambda) \quad (1)$$

where L is the thickness of the layer and λ is given by

$$\lambda = [\zeta/(\chi_1 + \chi_2)^{1/2}] \quad (2)$$

The quantities χ_1 and χ_2 in eq 1 are impedances per unit of length corresponding to the whole electrode area A , and their impedance on frequency and/or position is determined by the transport properties in each phase, whereas ζ is an impedance length describing faradaic currents and polarization at the distributed interface. The model of eq 1 represented in the scheme of Figure 2a is formulated in terms of differential equations, according to refs 10 and 11, and some applications and discussions of the porous theory can be found in refs 12–14.

The model assumes that the dominant contribution to the current is the electrical field. The porous structure allows electrical current to spread in various directions. The electrical charge can flow along each medium, and the resulting ac currents are termed here \tilde{i}_1 and \tilde{i}_2 (the subscripts 1 and 2 denote the solid and liquid phases, respectively). They follow the x direction in the scheme of Figure 2a; that is, both \tilde{i}_1 and \tilde{i}_2 are *parallel* to the inner surface due to electrochemical reactions and/or capacitive charging. Therefore, at a given location, \tilde{i}_1 may decrease (increase) with a corresponding increase (decrease) of \tilde{i}_2 , with the constraint being obeyed that $\tilde{i}_T = \tilde{i}_1 + \tilde{i}_2$ (the total current flowing through the external circuit) is independent of position). It can be noted that the overall impedance of eq 1 is isomorphous to that of the transmission line (Figure 2a). With regard to the distribution of electrical potential, the simple assumption is made that an ac potential can be defined in each phase $\tilde{\phi}_1$ and $\tilde{\phi}_2$ which is, at each frequency, a unique function of position x ; no radial distribution of potential into the pores or solid phase is considered. It follows, therefore, that the ac potential difference between the two phases at a point x , that is, the overvoltage in interfacial reactions, is $\tilde{\phi}_1 - \tilde{\phi}_2$.

In the specific case discussed here in regard to nanostructured electrodes for application in energy storage technologies, the first aspect to be noted is the fact that a restricted margin of variation of the steady-state voltage may cause the solid phase to alternate between significantly different behaviors, that is, from an insulating configuration to good electronic conductivity. The state-of-charge is another important parameter to be considered here, and consequently, the relaxation function under discussion takes on distinct shapes and forms. Therefore, our discussion of the porous electrodes theory is based on Li ion host materials with nanoscale-based structures, and the characterization of the relaxation function is addressed as a function of the most relevant parameters.

As a result, on the basis of the transmission line approach described by eq 1 and schematically represented in Figure 2a, it can be assumed that channels 1 and 2, represented by the generalized elements χ_1 and χ_2 , are purely resistive and associated with the transport of electronic and ionic species, respectively. Consequently, the electronic conductivity of the solid phase is well described by a distributed resistance

$$\chi_1 = r_1 = \frac{1}{A\sigma_e} \quad (3)$$

where A is the geometric surface of the phase and σ_e is its electronic conductivity. Assuming that the Nernst–Einstein relation is obeyed, the conductivity is related to the diffusion coefficient, D_e , by the equation

$$\sigma_e = \frac{q^2 \bar{n}}{k_B T} D_e \quad (4)$$

where \bar{n} stands for the dc concentration of electronic charge carriers, q is the elementary charge, k_B is Boltzmann's constant, and T is the temperature. Therefore, in this simple model (Ohm's law) the conductivity is solely a function of the local concentration of carriers and the diffusion coefficient of the material. No other anomalous transport effects will be considered in the present analysis. Thus, the total contribution to the resistance (Ω) distributed in this phase is given by

$$R_1 = Lr_1 \quad (5)$$

A similar situation can be considered for the liquid phase (flooded pores) $\chi_2 = r_2$, representing the ionic transport throughout the channel flooded with liquid electrolyte, with the total resistance given by $R_2 = Lr_2$. Finally, for the sake of simplicity, we will assume that the transverse impedance element ζ obeys the ideal Debye relaxation model,¹⁵ as shown in Figure 3a and b, which is dependent on the frequency, as shown below:

$$\zeta^{-1} = i\omega C_{dl} + \left(R_{ct} + \frac{1}{i\omega C_b} \right)^{-1} \quad (6)$$

or in ref 15

$$\zeta^{-1} = \left[C_{dl} + C_b \frac{1}{1 + (i\omega/\omega_t)} \right] i\omega \quad (7)$$

where $\omega = 2\pi f$ and $\omega_t = 1/(R_{ct}C_b)$.

On the basis of eqs 6 and 7, it is assumed that a potential difference exists in the region between the two phases, which is sustained by the charge stored at the interface, as in the ideally polarizable interface. Therefore, C_{dl} is the interfacial capacitance attributed to the double-layer effects. The C_{dl} , in the present case, is described as being parallel with a $R_{ct}C_b$ series circuit (Figure 3b). The R_{ct} is stated as the classical heterogeneous charge transfer at the solid/solution interface, which is the transition of S Li⁺ ion site in the double layer to the B (bulk) sites inside nanocrystalline materials, as illustrated in Figure 4. The capacitance C_b stands for the charging of Li⁺ ions into nanocrystalline bulk sites, as schematically represented in Figure 3a and b. In this analysis, C_{dl} compensates the electron's charge at the interface, while the C_b compensate the electron's charge inside the bulk to meet the requirements of electroneutrality. Thus, C_{dl} is a capacitance representing a nonfaradaic process, while C_b is a capacitance describing a faradaic process.

III. Nanoscale Charging and Kinetics

A. Nanoscale Effect on Ion Diffusion. The arguments for the choice of a single capacitance to represent the Li⁺ bulk charging are given in this section. The primary argument is that, on a nanoscale, the kinetic limitation associated with the transport of ions in the lattice—this transport basically being controlled by diffusion resistance—is overcome more easily the smaller the nanoscale for diffusion, so that the characteristic diffusion frequency cannot be determined on the basis of the range of frequencies commonly used in frequency-dependent

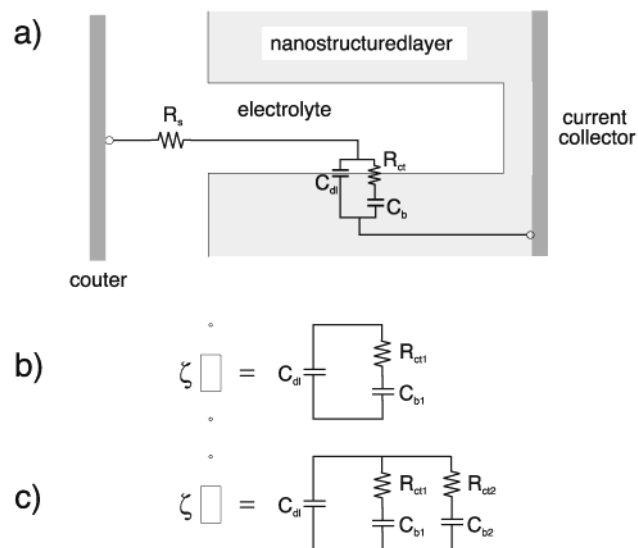


Figure 3. Schematic representation of distinct Li^+ ion modes of charging a nanostructured electrode, as discussed herein: (a) charging when the electronic and ionic transport are fast; (b) interfacing circuit element when only one kind of intercalation site is present; (c) interfacing circuit element when two intercalation sites exist (with distinct insertion energies).

techniques. In other words, diffusion through the approximately spherical nanosized particle or through the radius of a nanofiber is fast enough, in terms of the modulated frequency, to allow the concentration to remain virtually at the equilibrium level, even as the potential varies with time.

Strictly speaking, a cylindrical or spherical geometry should be considered.¹⁶ However, for the sake of clarity, a spatially restricted diffusion impedance, which shows two distinct regimes of behavior with respect to the characteristic frequency of transient time D/r^2 , can be used as a simpler example to better elucidate what was described in the previous paragraph (with a good approximation and without causing major error in the analysis, because a nanometer scale of diffusion is being

considered). Accordingly, the length for diffusion, at a distance r of a few nanometers, reduces the diffusion impedance response to the so-called diffusion capacitance.¹⁷ In other words, the charging process along a nanosized particle (or a nanofiber) can be represented by a capacitance or a simple capacitive element in an analogy with equivalent circuits. In fact, this is because the ordinary description for diffusion provides an equilibrium intercalation capacitance. Consequently, it could be argued that, in a nanoscale structure, since Li^+ must diffuse in a restricted radius (short path), the equilibrium concentration is reached quite rapidly, despite the diffusion resistance. The characteristic frequency of diffusion, considering a value of $D = 10^{-8} \text{ cm}^2 \cdot \text{s}^{-1}$ and a 10 nm diffusion length, is calculated as 10^5 Hz .

It should be noted in a scenario such as the one described, which takes place in nanostructured insertion electrodes based on spherical-like particles or nanofibers, that the liquid phase is also very important and may penetrate in large amounts inside the film, covering the particles' surface as much as possible to ensure the "nanoscale effect" throughout the electrode's thickness. From an experimental viewpoint, this condition can be reached easily using the smallest possible particle size or a template synthesis for nanofiber fabrication, to form a more effective liquid (electrolyte) connected channel, particularly in the case of nanofiber-based electrodes. Furthermore, when the liquid phase is highly conductive owing to a strong concentration of Li^+ ions, it is expected that, in a nanostructured porous configuration, the Li^+ ions in the double layer are exchanged for those in the nanoscale bulk, so that $1/(R_{ct}C_b)$ acts as an ion-trapping/release relaxation frequency. In this situation, it must be kept in mind that the intercalation concentration is in equilibrium with the Li^+ ion in the compact layer of the double layer region.

Therefore, when the proper conditions exist for fast transport in both the solid and liquid phases, as in the diagram of Figure 3a, or when the electrode is in a state-of-charge ($C_b \gg C_{dl}$), as in the diagram of Figure 2b, a relaxation process is predicted and a characteristic frequency corresponding to ω_t is identified,

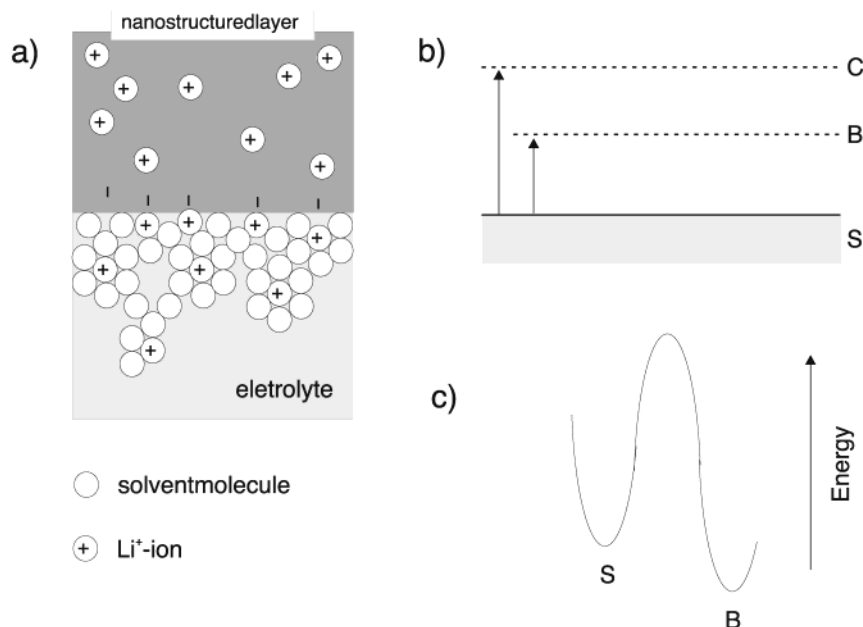


Figure 4. Schematic representation of the immobilization process from the solution phase to the bulk. (a) Representation of the interface between the solution and the solid phase, obeying requirements of electroneutrality in a nanoscale region. Parts b and c represent the "diagram" of the energy of available sites for intercalation in the lattice. Note that S is the solution site and B and C are intercalation sites. C sites are not represented in part a or c.

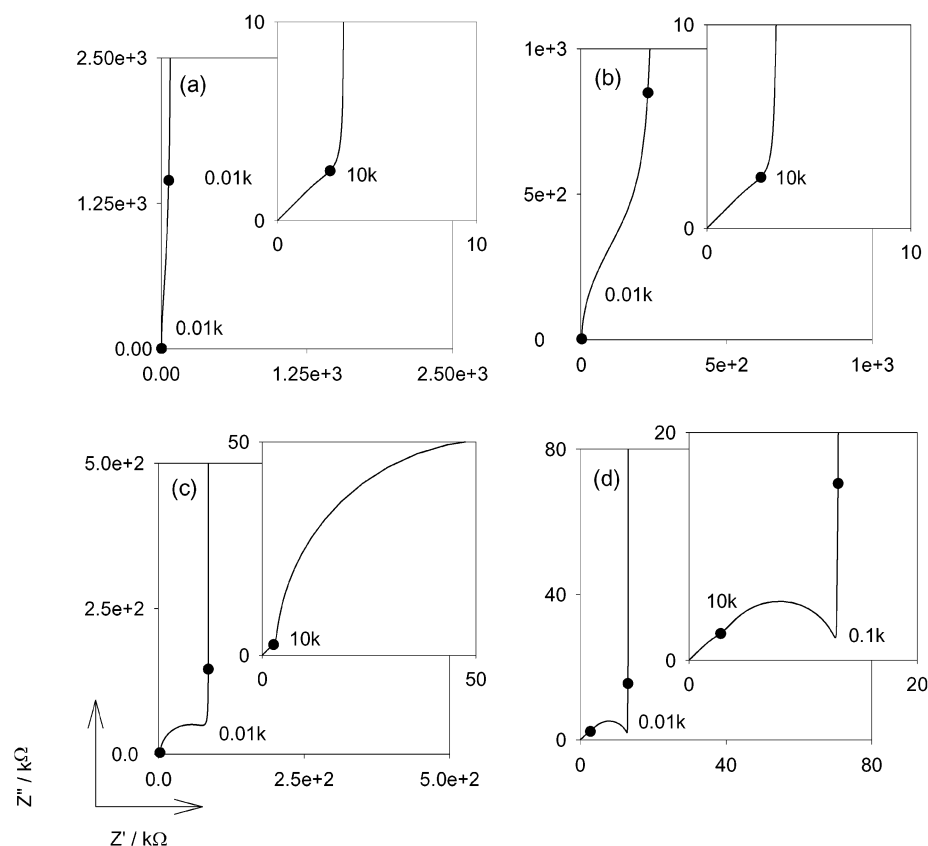


Figure 5. Illustration of the frequency-dependent impedance ($Z^* = Z' + iZ''$) for a single immobilization level in different states-of-charge. The immobilization site or trap has a characteristic frequency, $\omega_t = 0.01 \text{ rad}\cdot\text{s}^{-1}$, and a resistance, $R_{tc} = 1/(\omega_t C_b)$ with C_b changing from (a) $C_b = 0.1 C_{dl}$ to (b) $C_b = 1.0 C_{dl}$ to (c) $C_b = 10 C_{dl}$, to (d) $C_b = 10^2 C_{dl}$. C_{dl} has the value $10 \mu\text{F}$ in this representation. The insets represent the high-frequency region of the spectrum. All the frequencies marked are in millihertz. The points correspond to characteristic frequencies of diffusion ($\omega_d/2\pi \sim 10 \text{ Hz}$) and trapping ($\omega_t/2\pi \sim 0.01 \text{ Hz}$), respectively.

so that C_{dl} and C_b capacitances are graphically obtained from the complex capacitance plane.

B. Charging with Simple Transport. So far, a model was suggested in which the Li^+ diffuses through the bulk so rapidly that it does *not* influence the Li^+ frequency response. On the basis of these properties of the model, it is important now to verify the behavior expected when the dc resistance of the nanocrystalline materials is high enough to influence the frequency response and to overlap, to some extent, the trapping ion response. It was also considered that the resistance for Li^+ transport through the electrolyte channel (porous) is sufficiently low *not* to cause a drop of the potential in the porous channel. Experimentally, this can be achieved easily with a supporting electrolyte. Therefore, the channel represented by r_2 was considered to be in a short-circuit situation.

Thus, Figure 2b portrays the case that will be discussed in this section, while r_1 given in eq 5 represents the dc resistance of the nanocrystalline material to electronic transport. r_1 is present in most nanocrystalline metal oxides (semiconductors) used in nanostructured insertion electrodes. The main features of the impedance frequency responses of such cases are shown in Figure 4. Here, the C_b is expected to increase with a negative overpotential. For the sake of simplicity, the frequencies of the trap state ω_t and electronic transport $\omega_d = 1/(R_1 C_{dl})$ were considered constant and the changes in the pattern of frequency responses are only due to variations in C_b with the steady-state condition or with the state-of-charge of the insertion materials. The impedance representation in Figure 5a and b displays a quasi-vertical line at frequencies lower than $\omega_d/2\pi$ and a Warburg impedance at frequencies higher than the correspond-

ing frequency. This is a consequence of the lower C_b state-of-charge with a slight influence of the ion-trapping state in the impedance response.

At a higher C_b state of charge, the trapping state starts to dominate the frequency responses, as illustrated in Figure 5c and d. At this state-of-charge, the ω_t marks the transition to an arc at high frequency, corresponding to the parallel coupling of the heterogeneous charge-transfer resistance R_{tc} and double layer capacitance C_{dl} : $R_{tc}C_{dl}$. The predominance of C_b over the system's total capacitance $C_{dl} + C_b$ is well illustrated in Figure 6, which shows the complex capacitance response and clearly identifies of the immobilization or trapping relaxation. When $C_b > C_{dl}$ (Figure 6c and d), its value is obtained by the width of the capacitance arc. At higher frequencies, C_{dl} shifts the arc to the right, to the extent corresponding to its value.

The state-of-charge and the influence of the trapping state on the frequency responses when simultaneous effects of transport and trapping processes are present can also be seen by frequency-resolved capacitance (in a log-log plot) of both real and imaginary parts, as shown in Figure 7. This figure shows that the transport process strongly affects the responses at frequencies above 10 Hz. However, the influence of the transport process continues gradually up to frequencies of about 0.1 Hz. The relaxation process observed in Figure 7a at 10 Hz is due to $\omega_d/2\pi$, and its influence tends to decrease with the system's state-of-charge. At a higher state of charge, the relaxation process (0.01 Hz) caused by $\omega_t/2\pi$ begins to prevail, and, in the C' versus frequency plot, the C_{dl} and C_b values are clearly separable.

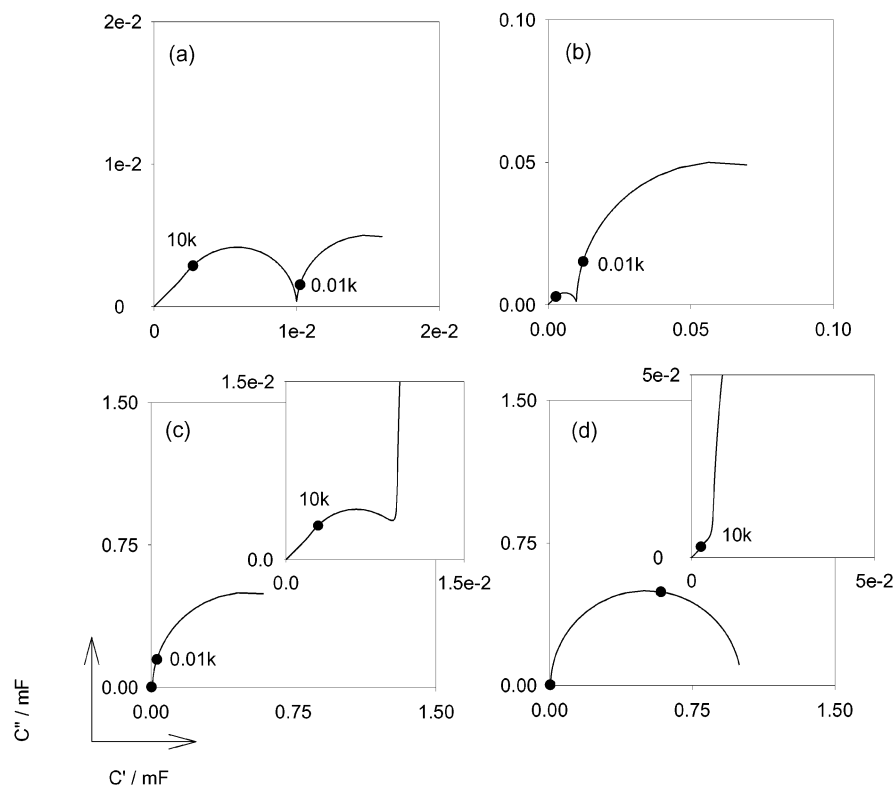


Figure 6. Illustration of the frequency-dependent capacitance ($C^* = C' + iC''$) for a single trap level at different states-of-charge. The trap has a characteristic frequency $\omega_t = 0.01 \text{ rad}\cdot\text{s}^{-1}$ and a resistance $R_{tc} = 1/(\omega_t C_b)$ with C_b changing from $0.1C_{dl}$ up to $10^2 C_{dl}$: (a) $C_b = 0.1C_{dl}$; (b) $C_b = 1.0C_{dl}$; (c) $C_b = 10C_{dl}$; (d) $C_b = 10^2 C_{dl}$. C_{dl} has the value $10 \mu\text{F}$. The insets represent the high-frequency region of the spectrum. All marked frequencies are in millihertz. The points correspond to characteristic frequencies of diffusion ($\omega_d/2\pi \sim 10 \text{ Hz}$) and trapping ($\omega_t/2\pi \sim 0.01 \text{ Hz}$).

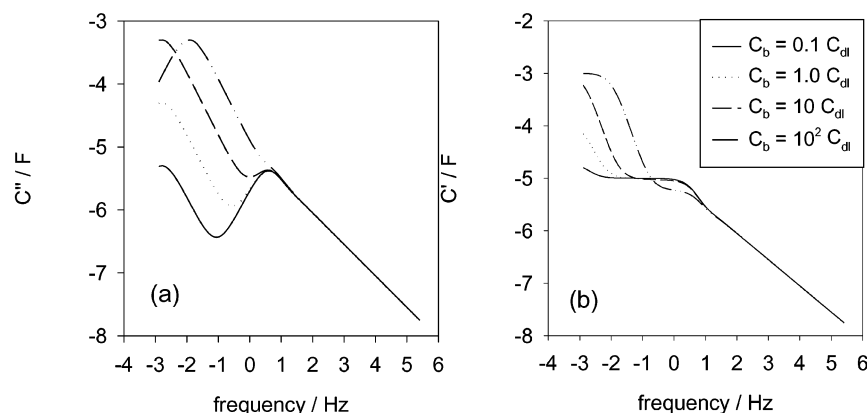


Figure 7. Capacitance C^* spectra illustrating the influence of state-of-charge of C_b : (a) real and (b) imaginary parts. The trap has a characteristic frequency $\omega_t = 0.01 \text{ rad}\cdot\text{s}^{-1}$ and a resistance $R_{tc} = 1/(\omega_t C_b)$ with C_b changing from $C_b = 0.1C_{dl}$ to $C_b = 10^2 C_{dl}$. C_{dl} has the value $10 \mu\text{F}$.

In regard to this frequency response representation, it is important to check the frequency range in excess of 10 Hz for diffusional effects. These effects seem to dominate the response when the layer is at a lower state-of-charge, mainly when $C_{dl} \geq C_d$ in the films, as inferred from the high-frequency interval of the impedance spectra. However, in the case of $C_b > C_{dl}$, at a lower frequency interval, the response of porous nanostructured films is determined exclusively by the trapping mechanism.

C. Charging with Fast Transport. We now discuss the case of fast electronic transport during charging of nanocrystalline-based electrodes. As we shall see, a Debye or other more complicated relaxation process is expected to appear in the frequency-based response when the influence of transport due to electronic carriers is weak. Fast electronic transport can be achieved experimentally by doping a nanocrystalline metal oxide semiconductor, thereby increasing the donor density, as will be

discussed in part 2. In the scheme of Figure 3a it is equivalent, in an ideal case, to short circuiting the channel formed by the solid phase, leading to the scheme of Figure 3b. In this case, no Warburg-like response is expected to arise at high frequencies, contrary to what was observed in Figures 5 and 6. The capacitance of C_{dl} , for instance, should be easily observed and separated from the electronic transport process. In other words, in this case, the nonfaradaic and faradaic capacitance-related processes can be more clearly separated, even at a lower C_b state-of-charge. Furthermore, in this condition, the presence of more than one ion immobilization or trap state is visible. The responses are not simulated here because it is very common and quite simple to be predicted.¹⁵

D. Basic Kinetic Aspects. 1. Li^+ Fast Charging State: Nonfaradaic Process. We propose here a model system in which connected porous paths are available for the solvated Li^+ to

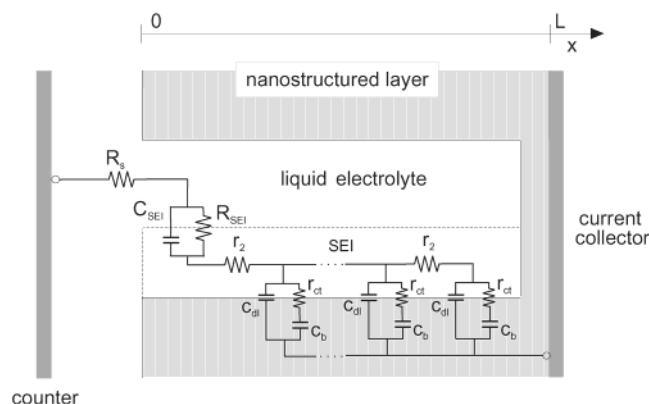


Figure 8. Schematic representation of the inner region $0 < x < L$ of a nanostructured electrode, consisting of a porous film deposited on a conducting substrate in whose inner porous region a solid electrolyte interface (SEI) is formed. The R_{SEI} represents the ion transport properties from liquid electrolyte into solid electrolyte film, and C_{SEI} represents the capacitance of the SEI, respectively. The dashed line indicates the solid/liquid and solid/solid interfaces inside the pores. The figure illustrates the approximately equivalent circuit model when the SEI is formed. Note that the scale used is illustrative. In the specific case of nanostructured electrodes, the thickness of the SEI is expected to be dozens of times greater than the ion diffusion length in the host material. The nanostructure does not have to be as regular as the one depicted here (for a detailed explanation, see section 2), but each phase must be continuous throughout the electrode's length.

fill the inner layer of nanosized particle surfaces uniformly throughout the L electrode's thickness. It should be clarified that, in this model, *specifically adsorbed* and/or solvated Li^+ ions are assumed to be exchanged with the diffuse layer of the electrical double layer, in a dynamic *equilibrium*.

The number density of Li^+ ions in a compact layer can therefore be denoted as n_{dl} . Note that any restriction preventing *specific adsorbing* and/or solvated Li^+ ions from reaching the compact layer is avoided and the occupancy of the n_{dl} sites, during time transients or frequency measurements, is an equilibrium value which is determined by the electrode's potential at each moment. In other words, we affirm here that the kinetics of the nonfaradaic process is very rapid and any excess charge in the electronic conducting phase can be compensated by Li^+ at the surface or intercalated Li^+ ions, which is an obvious consequence of what was stated in the previous sections. Therefore, the sheet of charge, having opposite polarity at the surface (double layer), is equivalent to a parallel-plate capacitance, which can be defined as

$$C_{dl} = \frac{d\bar{Q}_{dl}}{dV} = e \frac{\bar{n}_{dl}}{dV} \quad (8)$$

Consequently, C_{dl} is a differential capacitance that can be predicted by models for double-layer structures. Here, therefore, if the function $\bar{n}_{dl}(\bar{V})$ is assumed to be the simplest case of the Boltzmann statistics,

$$n_{dl} = n_0 \exp(-eV/k_B T) \quad (9)$$

where n_0 is the concentration of ions in the diffuse layer or solution bulk, then the form of the C_{dl} capacitance is

$$C_{dl} = \frac{e^2}{k_B T} n_{dl} \quad (10)$$

which increases exponentially as the electrode's potential becomes more negative. The reason for this unlimited rise in

differential capacitance of eq 10 with negative potential is that, in the present case, the ions are not restricted in terms of their location in the compact layer. They are considered as point charges that can approach the surface arbitrarily closely. Thus, as a result of this mathematical treatment, at high polarization, the effective distance separating the solid- and solution-phase charge zone decreases continuously toward zero. This view is far from realistic, because the ions have a finite size and cannot approach the surface any closer than the ionic radius. Therefore, if the ions remain solvated, the thickness of the primary solution sheath would have to be added to that radius and an increment might be necessary to account for a layer of solvent on the electrode's surface, allowing one to envision a plane of closest approach for the center of the ions at some distance. In this scenario, it can be established that the compact layer may have a limited occupancy that defines the maximum value of n_{dl} . This will be particularly important to predict the capacitance of C_{dl} in a high electrolyte concentration of Li^+ . In the classical model of the Gouy–Chapman–Stern model for double-layer structures, C_{dl} in a larger electrolyte concentration predicts the capacitance of the charges held in the compact layer of the double layer, which, in some situations, can be independent of the potential and assumed to be constant.

In future developments it will *not* be necessary to assume a specific form for the occupation function of the ions in the double-layer structure which, in the present model, describes what has been dubbed the fast nonfaradaic charge process. However, a good candidate to describe the differential capacitance of the double layer is the one predicted by the classic Gouy–Chapman–Stern model.

2. Li^+ Slow Charging: Faradaic Process. Now it is believed that the ion charge in the nonfaradaic fast state does *not* exhaust the possibilities of neutralizing electronic charges in the solid phase, and another type of site is assumed to exist, besides those in the compact layer, which is more difficult for Li^+ to access. These difficult-to-access sites may be filled with ions originating from the fast state sites of the nonfaradaic process, as illustrated in the scheme represented in Figures 2b and 3a and discussed in the previous two sections. Accordingly, the scheme of Figure 4a represents the Li^+ ion insertion into a crystalline host structure consisting of a nanostructure with a spherical particle- or fiber-based geometry. This nanostructure leads to a similar boundary condition to the one described in ref 18, in which this lower ultimate charging state is considered as an ion-trapping state because the distance that Li^+ must diffuse is very short in nanostructured electrodes, leading to a pure capacitive response, as previously discussed. However, the fast charging state described here is a nonfaradaic process with a capacitance corresponding to a value close to that of the double-layer capacitance. Here, the Li^+ in the double-layer structure mediates the Li^+ between the solution and the ion-trapping state modes existing in the bulk material. Conversely, in the case of ref 18, the equilibrium dynamics of the trapping state occurs between two solid-state sites with a homogeneous charge transfer, which is, therefore, physically different from the one proposed here. The model of ref 18, for instance, could be applied to a homogeneous and nonporous layer, such as the one developed in ref 19, in agreement with ref 18.

Consequently, the equilibrium here occurs between intercalated and surface Li^+ ion sites. Therefore, the n_b , which is the density of intercalated Li^+ ions, is related to the composition by $x = n_b/N$, where N is a number density proportional to the host's nanosize, such as the density of one type of site or intercalated Li^+ ion (i.e. Li_xSnO_2 , $\text{Li}_x\text{Mn}_2\text{O}_4$, or Li_xCoO_2).

Therefore, n_b can be related to approximately C_b by the following expression:^{8,18}

$$C_b = -\frac{d\bar{Q}}{dV} = -re\frac{d\bar{n}_b}{dV} \quad (11)$$

where $Q = rn_b e$ and r is the radius of the nanoparticle or nanofiber.

The lattice gas model²⁰ is a widely used approach to describe the occupation of sites in a host material as a function of the electrode's chemical potential, which is known to change with the circuit voltage.^{8,9,11} Considering a model that neglects the ions' interaction and electronic contributions to the chemical potential and that assumes equivalent intercalation sites with concentration N and energy E_0 , the chemical potential can be given by refs 9 and 11

$$\mu = E_0 + k_B \ln\left(\frac{n_b}{N - n_b}\right) \quad (12)$$

Hence, C_b at equilibrium is described approximately by

$$C_b = \frac{re^2}{k_B T} n_b \left(1 - \frac{n_b}{N}\right) \quad (13)$$

where $Q = rn_b e$ and r is the radius of the nanoparticle or nanofiber. A more precise definition of eq 13 can be found in ref 18.

3. Equilibrium between Nonfaradaic and Faradaic Li^+ States. As discussed earlier, the charging of nonfaradaic fast states at the interface immediately follows the applied potential. However, in the present model, the total charge passed on to the porous film is *not* compensated only by interfacial states but also by a trapping bulk described by the incorporation of Li^+ into specific sites in the host structure. In such a scheme, the total capacitance resulting from charging the film is always $\geq C_{\text{dl}}$ because Li^+ ions can be largely inserted into the host structure to compensate charge. Hence, the kinetic *equilibrium* is maintained by transition of these ions to both interfacial and bulk-class sites. The relationship between the capacitances of bulk states and surface states is given by $\bar{n}_b = \bar{n}_b(n_{\text{dl}})$,¹⁸ implying that the steady-state value, n_b , is determined by the electrode potential V . The equilibrium is determined by the $S \leftrightarrow B$ transitions represented in Figure 4a and c. Accordingly, the total capacitance is given by

$$C_t = C_{\text{dl}} + C_b \quad (14)$$

4. Li^+ Intercalation and Deintercalation Rates. In the simplest case, where the C_b can be treated as a pure capacitance due to the "nanoscale effect" of diffusion media, a kinetic framework to describe the intercalation reaction can be developed similar to that of ref 18. Therefore, the sites for intercalation can be viewed as trapping-ion sites, and a trapping/detrapping approach (intercalation/deintercalation) is established between the intercalation sites in the bulk and (*specifically adsorbed*) (and/or solvated) the double layer. The occupation density $0 \leq n_b \leq N$ of intercalation states uses the kinetic constants β for intercalation and ϵ for deintercalation from the surrounding double layer. The time dependence of n_b is formulated as the balance equation

$$\frac{\partial n_b}{\partial t} = \beta n_{\text{dl}}(N - n_b) - \epsilon n_b \quad (15)$$

In eq 15, the insertion occupancy in the steady-state is given by

$$\bar{n}_b = \frac{\beta N n_{\text{dl}}}{\beta \bar{n}_{\text{dl}} + \epsilon} \quad (16)$$

Equation 16 can be solved in the way described in ref 18, so that

$$C_b = \frac{\epsilon}{\beta N} \left(\frac{\bar{n}_b}{\bar{n}_{\text{dl}}}\right) C_{\text{dl}} \quad (17)$$

According to eq 7, the total admittance of the circuit representing the trapping state by a Debye-type relaxation (Figure 3a and b) is given by $\zeta^* = i\omega C_t^*$, where C_t^* is the total complex capacitance. Thus

$$C_t^* = C_{\text{dl}} + C_b \frac{1}{1 + (i\omega/\omega_t)} \quad (18)$$

and

$$C_t^* = C_{\text{dl}} + C_b^* \quad (19)$$

According to eq 18 and eq 16 from ref 18, ω_t is defined as

$$\omega_t = \beta \bar{n}_{\text{dl}} + \epsilon \quad (20)$$

which is the characteristic frequency of the intercalation process and can be obtained easily from complex capacitance graphs, as was presented in sections 3.2 and 3.3.

E. Intercalation Reaction as an Ion-Trapping State. The characteristics of heterogeneous charge transfer in nanoscale materials and the equilibrium between bulk and surface sites for Li^+ ions, as discussed previously, are based on the premise that the insertion can be treated as a pure differential capacitance and that the ion diffusion takes place faster than the ac perturbation. Therefore, in nanoscale host materials, the ions are considered to be immobilized in certain sites, or intercalation sites, and the capacitance of the ion trap is considered to be only a contribution of the intercalation sites.

In metal oxides, for example, positive guests such as Li^+ occupy sites surrounded by negative oxygen ions, and they distance themselves as far as possible from the positive transition metal ions.²⁰ Since Li^+ has a filled outer core of electrons, the geometry of the site is not important, provided the anions are distributed evenly around the site. Thus, Li^+ surrounded by four anions would prefer to form a tetrahedron rather than a square in metal oxides. Moreover, in highly charged insertion composites based mainly on metal oxides, the guests spend most of their time localized on a given site, only occasionally hopping from one site to another (diffusion).

The sites available for ions depend on the structure, and a given structure can contain different types of sites, for instance, octahedral sites (surrounded by six oxygen anions) and tetrahedral sites (surrounded by four oxygen anions). Li^+ ions generally prefer to occupy these two types of site. The sequence of occupation of the sites depends on how the sites are connected (the channel formed by connected sites and the interaction between the different channels).

1. Electronic and Ionic Charging. It is important to point out that the model presented herein considers that the only contribution to ion trapping (or intercalation) capacitance is given by the Li^+ injected into the nanocrystalline structure of the host to compensate electrons from the current collector. In

other words, the injected electrons do *not* contribute to the intercalation capacitance. However, it is possible to assume that the dynamics of electrons follows that of ions, provided the occupation functions of the electrons and ions are the same or similar. This picture is particularly important to understand the relationship between Li^+ inserted charge and changes in the electronic structure, which are evidenced by electrochromic features or infrared absorption of hosts during intercalation.^{1,19,22}

Therefore, on the basis of several approximations, it can be considered that, for a metal oxide nanocrystalline host, the electron states introduced by the current collector to compensate Li^+ intercalated ions first occupy an empty d band. However, the Li^+ intercalated ion introduced to neutralize this electronic charge polarizes the oxygen anions around it and these, in turn, affect the neighboring metal ions, lowering the energy of their d states. This lowering of energy of d states around the neighboring metal of the intercalated ion site can pull states out of the band, localizing electrons until a high concentration of intercalated ions is reached. Nevertheless, situations other than the above-mentioned one may occur, as discussed in refs 9, 18, and 19, where an equilibrium capacitance (a fast charging state, in such cases) might arise without contributing directly to coloring centers, since the ions in such sites do *not* interact with the structure (they are free diffusion sites).

Considering only the first situation discussed here, in which every electron injected polarizes an oxygen atom in the structure, it can be established, according to the ion trapping scheme discussed in the preceding sections, that C_b is related to the intercalation reaction. If the host is an electrochromic material, with ions fully contributing to the coloring reaction, its kinetics depends strongly on the trapping dynamics of inserted ions.^{19,22} Therefore, the electrochromic efficiency, which is defined as the proportionality between the optical absorption change of the electrochromic material and the inserted charge density, similarly to the Beer–Lambert law, is proportional to the ratio $C_b/(C_{dl} + C_b)$, according to the kinetics discussed herein.

In addition, according to the intervalence charge transfer (IVCT)²³ and/or small polaron absorption²⁴ theories, which are the most widely accepted theories to explain the coloration occurring upon Li^+ insertion, this implies that electrons are required to be localized in quantum sites that are (energetically) below the conduction band (and said to be “valence trapped”), and the transitions between “valence trapped” and “nontrapped valence” would be responsible for absorption bands in the visible and near-infrared regions of the spectra.

As a result of the above picture, it can be concluded that intercalation sites (ion trapping) are capable of generating a “trapped valence” which is related to absorption bands in the visible or near-infrared region. It is even possible that the capacitance of the ion-trapping state may be used to monitor this optical change.

2. Distinct Ion Intercalation Sites. As explained earlier herein, a given lattice can contain two or more ion intercalation sites, depending on the thermodynamic properties of its structure. The thermodynamic properties can be altered according to the change of the composition with Li^+ insertion, as proposed in the lattice gas model theory.⁸ Accordingly, crystalline structures foresee the existence of more than one ion-trapping state, or intercalation reactions with distinct intercalation energies.²⁰ Therefore, a trapping scheme such as the one in Figure 4b is expected to arise, and another relaxation process may exist at a lower frequency. This new intercalation process may or may not contribute to optical absorption, but if it does, the mechanism should be similar to the one described in the previous section.

However, the kinetics of occupancy of these new sites may be more complicated than the one presented earlier for C_b . The occupancy of this ion-trapping state, for instance, given by a differential capacitance defined as C_c , should depend on the occupancy (or concentrations of ions) in the C_{dl} and C_b , particularly if the shallow (B) and deep (C) trap states interact. A study based on the *chemical potential* versus composition should be useful to provide this kind of information²⁰ in an experimental study. In frequency-resolved responses, a new trapping may be identified as a new relaxation process at a lower frequency. In crystalline structures, for instance, B-type ion-trapping sites are expected to be octahedral and C-type ones are expected to be tetrahedral.

In amorphous structures, a distribution of relaxation rates is more likely and the Cole–Cole relaxation function can be used to describe such a distribution, as exhaustively discussed in refs 18 and 19.

F. Effect of Solid Electrolyte Interface Formation. As discussed in the Introduction, the use of nanoscale materials in lithium ion storage devices or electrochromic windows represents substantial advantages because these materials offer successful solutions for improving the rate capability. Therefore, in the sections following the Introduction, we discussed a “nanoscale effect” in the frequency domain response of electrodes with porous nanoparticles or nanofiber geometries in which the Li ion diffusion restriction is overcome. The present section discusses the effect of a very important practical problem pertaining to the electrode’s covered active mass (surface film), that is, interfaces between the host nanoparticles or the nanofiber and the electrolyte solution, which is always involved.²⁵ Lithiated transition metal cathodes, lithiated intermetallic compounds, and lithiated carbons in nonaqueous solutions are usually covered with surface films that are formed either spontaneously or due to the electrode’s polarization. Hence, there is usually a necessary stage of ion migration through surface films, which traverses the solution phase and reaches the solid-state host.

We do not intend to make a detailed analysis of the SEI (solid electrolyte interface) theory²⁶ in this section, but we intend simply to discuss the effect its presence is expected to exert on the model previously discussed. As we shall demonstrate in this section, the surface film or solid electrolyte layer will introduce additional steps in the high-frequency region of the immittance spectrum. Therefore, a supplementary relaxation process is introduced in the frequency domain response. An impedance representation of this process will be seen as a semicircle, which reflects the ion transport properties and capacitance of the surface film. Figure 8 shows the equivalent circuit model of the effect of ion transport properties and capacitance of a surface film, which is a preliminary step for the mechanism discussed previously. As illustrated in Figure 8, it is worth noting that the presence of R_{SEI} and C_{SEI} does *not* affect the foregoing kinetic analysis, although they control the boundary values, such as the n_0 value and hence, according to eqs 9 and 10, the n_{dl} and C_{dl} values. In other words, the presence of a stable solid electrolyte layer represents the former liquid electrolyte, and a new double-layer structure between a solid host and a solid-state electrolyte must control the C_{dl} value in the solid–solid interface. The values of n_0 and n_{dl} depend on the composition of the solid electrolyte layer, since C_{SEI} must also be considered as a differential capacitance similar (but *not* necessarily equivalent) to those of eqs 9–11 and some measure of equilibrium between C_{dl} and the bulk capacitance of the SEI (C_{SEI}) is expected in the steady-steady condition. The R_{SEI}

represents the ion transport properties from liquid electrolyte into solid electrolyte film and *not* the resistance of the SEI itself, which is distributed along the pore's thickness, according to Figure 8.

It should be noted that, in the case of SEI formation, the presence of a potential drop (sketched in Figure 8, $\chi_2 = r_2$) in the solid electrolyte layer is expected because the ionic conductivity in solid state electrolytes is lower than that in liquid electrolytes. Hence, the potential drop cannot be avoided by using a supporting electrolyte. Particularly in the case of nanostructured Li ion electrodes, the formation of a SEI involves a film whose thickness is equivalent to or greater than the Li ion diffusion length in the host. The configuration of Figure 8 takes this feature into account and is appropriate for very electronically conducting hosts.

The representation of a solid electrolyte layer by means of a $R_{\text{SEI}}-C_{\text{SEI}}$ parallel circuit is a rough approximation which is used here simply to exemplify the effect of the SEI on the total frequency domain response. The surface layer is usually a multilayer structure which can be more accurately modeled by a "Voigt"-type analogue, as was discussed in refs 27–29.

Finally, it is worth noting that, in cases of low state-of-charge of the electrode with SEI formation, the immittance spectra must have low resolution concerning the Li ion insertion step so that relaxation processes due to SEI, double-layer capacitance, and charge-transfer resistance must prevail. Other cases of lower resolution owing to the Li ion insertion step must be related to the formation of highly resistive surface films caused by passivation with an inactive layer, sometimes leading to degradation of electrolyte species and thickening of the SEI during cycling.²⁵ On the other hand, under stable SEI conditions and with high state-of-charge of the electrode, the response of the SEI relaxation process to the overall impedance response (mainly in the low frequency region) must be lower, particularly because $C_b \gg C_{\text{dl}} + C_{\text{SEI}}$ under such conditions.

IV. Summary and Conclusions

In summary, it can be concluded that, during the insertion of Li ions into nanostructure-based electrodes, some sort of relaxation process is expected to arise in the domain response. The relaxation process is expected to be identified in the region of low frequency and is more likely to be visible in a higher state-of-charge of the electrode. However, under some circumstances, when the electronic conduction of the solid phase is sufficiently high, the relaxation process is expected to exist even at a lower state-of-charge.

The relaxation process originates from the existence of two distinct ion-charging modes, one much slower than the other (more difficult to access sites). We have called the slower one the ion-trapping state, and it involves the intercalation reaction of Li^+ in the host structure. Therefore, the nature of the relaxation process (or relaxation function) depends on the energy distribution of the intercalation sites.

In addition, the charging of the intercalation sites was modeled by a differential capacitance because the material's nanosize scale forms the nanostructure of the electrode. On the basis of

the porous electrode theory, an electrode composed of nanometer-scale material permits such a boundary condition and eliminates the need for an analysis of the diffusion resistance (the diffusion resistance does *not* respond to the ac perturbation), as discussed in this article. Therefore, the nanolength for ion diffusion exerts a strong effect on the domain response of nanostructured electrodes. In this paper, this nanoscale-related effect was dubbed the "nanoscale effect".

Finally, it can be concluded that the analysis described herein contributes to studies of the properties of nanoscale electrodes, by means of frequency response analysis, for lithium ion energy storage devices and electrochromics, whose most important feature is the effect of nanosize on solid-state diffusion. Part 2 of this series will report on the analysis of electrochromic SnO_2 nanostructured electrodes.

Acknowledgment. The financial support of this research project by the São Paulo research funding FAPESP is gratefully acknowledged. Special thanks are due Ms. Beatrice Allain for her grammatical correction of this text in LATEX format.

References and Notes

- (1) zum Felde, U.; Haase, M.; Weller, H. *J. Phys. Chem. B* **2000**, *104*, 9388.
- (2) Tarascon, J.-M.; Armand, M. *Nature* **2001**, *414*, 359.
- (3) Martin, C. R.; Li, N.; Scrosati, B. *J. Power Sources* **2001**, *97–98*, 240.
- (4) Nagasubramanian, G.; Jungst, R. G. *J. Appl. Electrochem.* **2001**, *31*, 99.
- (5) Li, N.; Martin, C. R.; Scrosati, B. *Electrochem. Solid-State Lett.* **2000**, *3*, 316.
- (6) Li, N.; Martin, C. R. *J. Electrochem. Soc.* **2000**, *148*, A164.
- (7) Paasch, G. *Electrochim. Acta* **1993**, *38*, 2653.
- (8) McKinnon, W. R.; Haering, R. R. *Modern Aspects of Electrochemistry*, vol. 15; Plenum Press: New York, 1983.
- (9) Bisquert, J.; Vikhrenko, V. S. *Electrochim. Acta* **2002**, *47*, 3977.
- (10) de Levi, R. *Electrochim. Acta* **1963**, *8*, 751.
- (11) Bisquert, J. *Phys. Chem. Chem. Phys.* **2000**, *2*, 4185.
- (12) Albery, W. J.; Elliot, C. M.; Mount, A. R. *J. Electroanal. Chem.* **1990**, *288*, 15.
- (13) Albery, W. J.; Mount, A. R. *J. Chem. Soc., Faraday Trans.* **1994**, *90*, 1115.
- (14) Candy, J.-P.; Fouillox, P.; Keddan, M.; Takenouti, H. *Electrochim. Acta* **1981**, *26*, 1029.
- (15) Böttcher, C. J. F. *Theory of Electric Polarization*; Elsevier: Amsterdam, 1978.
- (16) Jacobsen, T.; West, K. *Electrochim. Acta* **1995**, *40*, 255.
- (17) Bisquert, J.; Garcia-Belmonte, G.; Fabregat-Santiago, F.; Bueno, P. R. *J. Electroanal. Chem.* **1999**, *475*, 152.
- (18) Bisquert, J. *Electrochim. Acta* **2002**, *47*, 2435.
- (19) Bueno, P. R.; Garcia-Belmonte, G.; Fabregat-Santiago, F.; Bisquert, J. Submitted for publication.
- (20) Mattson, M. S. *Phys. Rev. B* **1998**, *58*, 11015.
- (21) Mackinnon, W. R. *Solid State Electrochemistry*; Cambridge University Press: Cambridge, U.K., 1995.
- (22) Fabregat-Santiago, F.; Garcia-Belmonte, G.; Bisquert, J.; Ferriols, N. S.; Bueno, P. R.; Longo, E.; Suay-Anton, J.; Castro-Garcia, S. *J. Electrochem. Soc.* **2001**, *148*, E302.
- (23) Faughnan, B. W.; Crandall, R. S.; Heyman, P. M. *RCA Rev.* **1975**, *36*, 177.
- (24) Schirmer, O. F.; Wittwer, V.; Baur, G.; Brandt, G. *J. Electrochem. Soc.* **1977**, *124*, 749.
- (25) Aurbach, D. *J. Power Sources* **2000**, *89*, 206.
- (26) Peled, E. *Li Batteries*; Academic Press: London, 1983.
- (27) Aurbach, D.; Zaban, A. *J. Electroanal. Chem.* **1994**, *367*, 15.
- (28) Aurbach, D.; Zaban, A. *J. Electrochem. Soc.* **1994**, *141*, 1808.
- (29) Aurbach, D.; Zaban, A. *J. Power Sources* **1995**, *54*, 289.